Electronic Structure of Mercury Oligomers and Exciplexes: Models for Long-Range/Multicenter Bonding in Phosphorescent Transition-Metal Compounds

Mohammad A. Omary,* Pankaj Sinha, Paul S. Bagus,* and Angela K. Wilson*

Department of Chemistry, University of North Texas, P.O. Box 305070, Denton, Texas 76203

Received: October 25, 2004

Spectroscopic and bonding properties of Hg_n oligomers and $^*Hg_n$ exciplexes are determined by rigorous theoretical treatments. Reliable values that agree well with experimental data have been computed for the luminescence energies and other molecular spectroscopic parameters by making a careful selection of theoretical methods and basis sets. The calculations clarified the assignments for several phosphorescence bands in the mercury vapor based on calculated energies and other parameters that quantify the large excited-state distortion in the emitting states. Both the weak ground-state mercurophilic bonding and the stronger covalent bonding in the triplet and quintet excited states studied are found to be cooperative, which is important for fundamental and applied research for luminescent and magnetic materials that have spectral behavior similar to that of Hg_n systems.

Introduction

Theoretical studies of the electronic structure and spectra of luminescent materials are of great significance for the design of better materials for technological applications. Theory can provide definitive assignments of the electronic states and the specific entities responsible for the emissions in existing luminescent materials as well as a priori predictions of the emission colors for new materials. However, rigorous characterization of the electronic structure of complexes containing heavy metal atoms has been difficult because of the size and complexity, including relativistic effects, of these systems. Largely on the basis of major advances in computational quantum chemistry and in the performance of modern workstations and supercomputers, it has become feasible to use theory to solve several puzzles in the photophysics of coordination compounds of heavy metals. Achieving this requires the coordination of the efforts of spectroscopists and computational chemists. While some success has been achieved in this regard, studies in which modern methods are used to compute the luminescence energies of transition-metal species remain relatively scarce.[1−4]

As a starting point in our ongoing efforts to model luminescent closed-shell transition-metal complexes of current interest (with d^{10}, d^8, and $d^{10}s^2$ configurations), we have chosen to pursue a study of the bonding and spectroscopy of mercury clusters. It is possible to study Hg_n species, at least for small to modest values of n, using several computational methods and large basis sets to describe the molecular orbitals (MOs). This allows us to validate the accuracy of our results with the different methods and to understand the consequences of the approximations that are used in the methods. This validation is particularly reliable because we are able to use the correlation-consistent series of basis sets for the MOs to systematically approach the complete basis set (CBS) limit at which the results are exact for the theoretical method used. For future work on larger models where more approximate methods must be used, our validations on the Hg_n species will enable us to make proper choices of methodology. However, since the Hg_n species have well-characterized spectral properties, the study of these systems has scientific value in its own right in addition to laying the ground for future studies of more complex systems. This scientific value has importance beyond the Hg_n systems since their bonding and spectral characteristics are similar to those in many of the aforementioned luminescent closed-shell transition-metal complexes. Common characteristics include weak ground-state metallophilic bonding,[5−10] covalent M−M bonding in many low-lying excited states leading to the formation of luminescent excimers and exciplexes,[11−21] the consequent very large Stokes shifts,[11−21] significant relativistic and correlation effects,[5] and the phosphorescent nature of the emission bands owing to a very large spin−orbit coupling.[7−25] In particular, the mercury dimer, Hg_2, is a simple vehicle to illustrate the chemistry underlying the properties of the ground and excited states that will be useful for the understanding of larger, more complex oligomers. A qualitative illustration of the spectroscopic and bonding features of the mercury dimer is shown in Chart 1. The transition from the antibonding orbital $\sigma_u^*{}_{(6s)}$ to the bonding orbital $\sigma_{g(6p)}$ results in an increase in the formal bond order from 0 in the $^1\Sigma_g^+$ ground state to 1 (i.e., a single bond) in the $^3\Sigma_u^+$ excited state. A low-energy excimer phosphorescence band results from the opposite transition.

In addition to the significance of closed-shell luminescent materials of coordination compounds in the aforementioned fundamental research areas, they have been receiving a great deal of attention in applied research in several different areas. These include photonics (e.g., molecular LEDs and laser materials),[26] nonlinear optics,[27] optical sensing of environmental pollutants,[28] solar energy conversion,[29] photocatalysis,[30] luminescent probes for biological systems,[31] optical telecommunication,[32] photoinduced magnetic switching,[33] optical writing,[34] and various inorganic conducting and semiconducting materials.[35] For the proper design of new materials for each of these technologies, understanding the electronic structure is extremely important. Hence, the experience gained in performing our studies of Hg_n species will be beneficial for future studies of

* To whom correspondence should be addressed. E-mail: omary@unt.edu (M.A.O.); bagus@unt.edu (P.S.B.); akwilson@unt.edu (A.K.W.).

10.1021/jp045143c CCC: $30.25
Published on Web 01/05/2005

CHART 1: A Qualitative Molecular Orbital Diagram for the Mercury Dimer

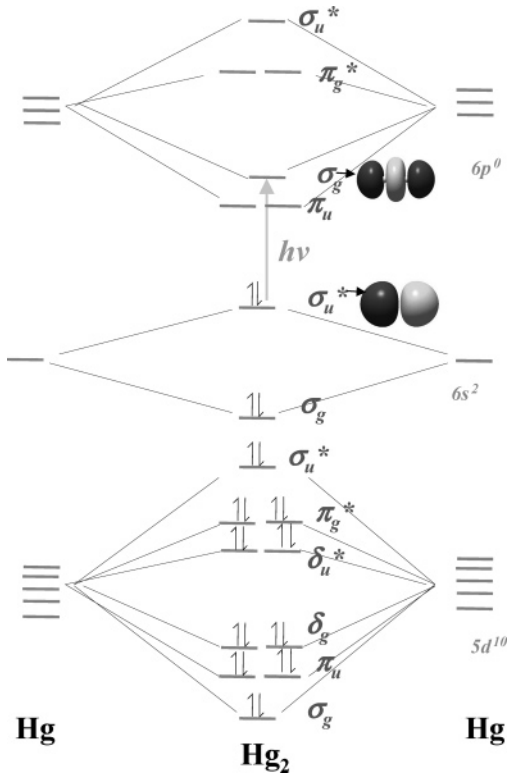

larger ligand-containing systems. In the cases of these larger systems, we will be able to select the most appropriate methodologies and approximations without the need to carry out a broad study with all the methods and basis sets used in the present work on the mercury species.

Since mercury vapor is known to exhibit bright continuum emissions with no nearby absorptions, it has long been proposed as a candidate for an excimer laser.[36] In fact, Cefalas et al. reported in 1986 a superfluorescent laser action based on molecular and atomic mercury species.[37] Two continuum phosphorescence bands are well-known to exist in the mercury vapor, a near-UV band centered at 335 nm and a green band near 485 nm.[38,39] These two bands are attributed to excited-state Hg−Hg bonded species.[38−43] The assignment accepted today relates the 335 nm phosphorescence to a $*Hg_2$ excimer, while the 485 nm band is related to a phosphorescent trimer exciplex, $*Hg_3$.[44] The efforts of computational chemists to improve the reliability of quantum mechanical calculations for mercury oligomers have been focused mostly on the ground state of the Hg_2 dimer molecule.[38,45−47] There are two noteworthy theoretical studies in which the excited states of Hg_2 were treated, both of which were concerned with constructing potential energy surfaces for a large number of excited states, including Rydberg states.[48,49] There are other theoretical studies of Hg molecular species before 1990, for which we refer the reader to the survey in ref 48. In the study by Czuchaj et al.,[48] only two valence electrons per Hg atom were treated explicitly (which means that the Hg 5d electrons cannot participate directly in the chemical bonding) and a semiempirical method was used to estimate the spin−orbit splittings. In the prior study by Balasubramanian et al.,[49] they considered somewhat fewer excited states of Hg_2 than those considered by Czuchaj et al.[48] and their basis sets for the valence orbitals were smaller. However, the theoretical treatment of Balasubramanian et al.[49] was, in some respects, more rigorous. In particular, they treated explicitly 12 valence electrons per Hg atom, thus allowing the 5d electrons to participate in the chemical bonding. Furthermore, for the excited states, relativistic wave functions were determined, and this placed the treatment of spin−orbit coupling and of electron correlation on an equal footing. Both these studies were restricted to the Hg_2 dimer.

In this paper, we address several issues in spectroscopy and bonding for Hg_n species with $n = 1$, 2, 3, and 4: (1) We assess the performance of a variety of theoretical treatments for accurate calculations of electronic transition energies. (2) We discuss the calculated luminescence energies in terms of the proper assignment of the continuum emission bands in mercury vapor. (3) We evaluate several spectral parameters that probe the extent of the geometric changes in the excited states of the various oligomers. (4) We study the cooperativity of the Hg−Hg bonding in the electronic ground state and the low-lying paramagnetic excited states that are relevant for the spectroscopy and bonding issues of concern. (5) We discuss the implication of the results on fundamental and applied research for closed-shell luminescent materials that have properties similar to those of the Hg_n species.

Computational Details

The calculations were performed for Hg_n ($n = 1-4$) species where all systems were assumed to be linear and to have $D_{\infty h}$ symmetry. For the trimer, the assumption that the molecule has $D_{\infty h}$ symmetry in its ground and excited states was tested and found to be correct. The theoretical methods used included coupled cluster with single, double, and quasiperturbative triple excitations, CCSD(T),[50] Møller−Plesset second-order perturbation theory, MP2,[51] and density functional theory, DFT, with the B3LYP and B3PW91 functionals.[52,53] The calculations were performed for the closed-shell ground states and for relevant low-lying paramagnetic excited states. Certain relativistic effects were included through the use of effective core potentials (ECPs) to represent core electrons that were not treated explicitly.[54] The relativistic effects included are those described as scalar relativistic effects[48,54] in contrast to spin−orbit coupling terms that are not treated. In this context, we note that the spin−orbit splittings are not expected to be especially large for the states of Hg_n of interest here; for example, for Hg_2, representative splittings for the low-lying excited states are <1000 cm^{-1}.[49] The closed-shell calculations were spin-restricted and were for pure singlets. The triplet and quintet states were spin-unrestricted and involved either unrestricted Hartree−Fock (UHF) wave functions or unrestricted density functional (UDF) densities. All calculations were performed using the Gaussian 98 suite of programs.[55]

Three types of combinations of ECPs and basis sets were used in this work: (1) A 12-electron ECP together with a double-ζ (DZ) quality contracted Gaussian-type orbital (CGTO) basis set. The ECP and CGTO parameters were optimized by Hay and Wadt.[56] Here, the 10 5d and the 2 6s electrons from each Hg atom are treated explicitly, while the remaining 68 core electrons are represented by an ECP. This ECP and basis set are available in the Gaussian library[55] under the descriptive name of "LANL2DZ". (2) A combination of ECP and basis set that was taken from the work of Couty and Hall.[57] An important feature of this combination is that CGTOs optimized to describe the atomic Hg 6p orbital have been included; otherwise, the basis set is of DZ quality. The Couty−Hall combination uses a 20-electron ECP developed by Christiansen and co-workers[58] so that the electrons arising from the $5s^25p^65d^{10}6s^2$ shells of each Hg atom are treated explicitly. ECPs such as this one avoid

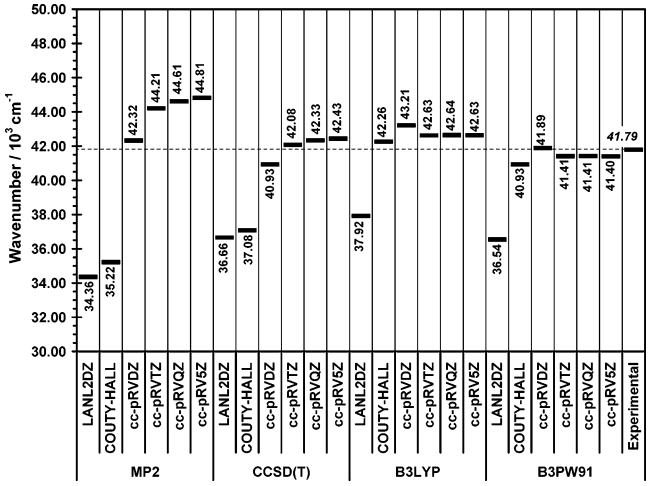

Figure 1. Calculated excitation energy for the atomic $^1S \leftrightarrow {}^3P$ transition in the Hg atom.

artifacts that can be associated with ECPs where fewer electrons are explicitly represented.[59] (3) A correlation-consistent (cc) series of CGTO basis sets known as the correlation-consistent polarized relativistic valence "*x*" ζ basis sets (cc-pRV*x*Z, where *x* is D (double), T (triple), Q (quadruple), and 5 (quintuple)) developed by Peterson.[60] These basis sets for Hg are based on a 20-electron ECP developed by the Stuttgart group.[61] The quality of this series of basis sets improves systematically with respect to increasing basis set size. As the basis set size increases, the CBS limit—the point at which the MOs are completely described, and no further improvement in basis set size will modify the results—is approached.[62,63]

For the calculation of the absorption and emission energies of the electronic transitions in Hg_n oligomers with $n \geq 2$, we consider vertical transitions between the singlet *gerade* ground state and the emitting triplet *ungerade* excited state. For the Hg_2 dimer, for example, the absorption energy is reported as the vertical transition energy at the position of the minimum of the $^1\Sigma_g^+$ ground-state potential energy curve while the emission energy is the vertical transition energy at the position of the minimum of the $^3\Sigma_u^+$ excited-state curve. For the dimer and trimer, our estimates of the Stokes shifts, the widths of the luminescence bands, and the excited-state vibrational quantum numbers are described in the next section. The vibrational and rotational parameters for Hg_n oligomers and $^*Hg_n$ exciplexes with $n \geq 2$ were taken from either frequency calculations for the optimized geometries of the models or a Dunham analysis[64] for a series of single-point calculations around R_e.

Results and Discussion

Electronic Transition Energies for the Hg Monomer. Figure 1 shows the results of the calculations of the excitation energies for the atomic $^1S \leftrightarrow {}^3P$ transition in the Hg monomer. Owing to the large spin−orbit coupling in the mercury atom, the three *J* levels of the ^3P state have large separation; the experimental values[65] are indicated in Chart 2, which shows the energy levels of the monomer in the presence and absence of spin−orbit coupling. When spin−orbit splitting and mixing are taken into account, the forbidden $^1S_0$ to $^3P_1$ transition becomes allowed because of the mixing of $^1P_1$ character into the dominantly $^3P_1$ state.[63] In Chart 2, we show schematically the effect of the configuration mixing between these two $J = 1$ levels by raising the position of the $^1P_1$ level slightly above the position of the ^1P term. This mixing also lowers the position of the $^3P_1$ level below that which would be given by the Landé

CHART 2: Electronic States of the Mercury Monomer in the Presence (Left) and Absence (Right) of Spin−Orbit Coupling[a]

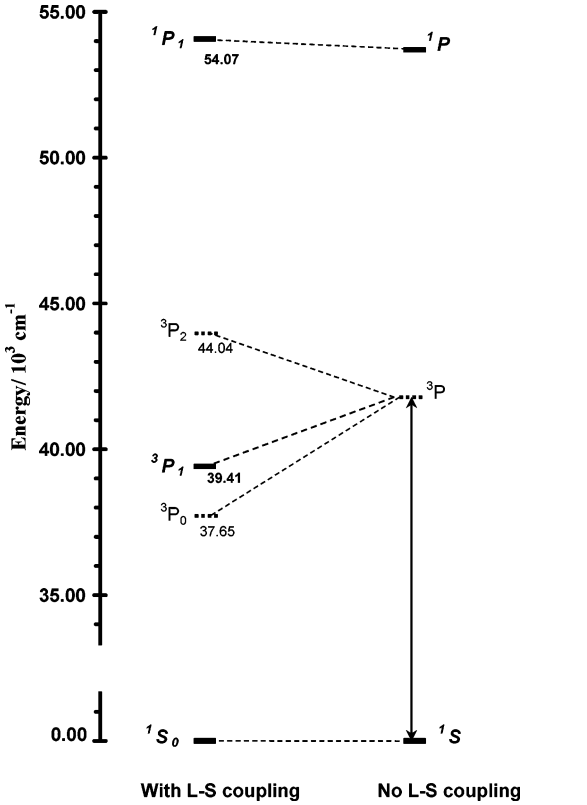

[a] Numerical values are according to ref 65. States involved in electric dipole allowed transitions are indicated in bold, while the arrow represents the transition calculated in Figure 1.

interval rule for L−S coupling in a pure ^3P term.[66] Although the deviation from the Landé interval rule is small for the ^3P level of the Hg atom, ~400 cm^{-1},[65,66] it is the small mixing of $^1P_1$ with $^3P_1$ that makes the $^1S_0$ to $^3P_1$ transition dipole allowed. Because spin−orbit coupling is not treated in the calculations performed in this work, the results are compared with the weighted average of the experimental values for the three $^1S_0 \leftrightarrow {}^3P_{2,1,0}$ transitions; we refer to this weighted average as the "experimental value" for the $^1S \leftrightarrow {}^3P$ transition. These monomer calculations serve to provide a calibration of the accuracy of the various theoretical methods and basis sets before their utilization to solve chemical bonding and spectroscopy problems for the dimer and larger Hg_n clusters. We have evaluated the performance of MP2, CCSD(T), and the DFT methods B3LYP and B3PW91 using the several basis sets and ECPs outlined above. These four methods account for electron correlation, which is extremely important for the various issues discussed in this work.[5]

The quality of the results was found to depend strongly on the basis set and ECP used. Figure 1 shows that the deviation from the experimental $^1S \leftrightarrow {}^3P$ transition energy was several thousand inverse centimeters with all four methods using the LANL2DZ basis set, which is conveniently available in the Gaussian suite of programs.[55] We conclude that using this standard basis set leads to qualitatively wrong results for transition energies of mercury species. The larger size of the Couty−Hall basis set and the inclusion therein of the outer 6p functions of Hg (which should be important for the excited states of Hg_n systems) as well as the use of a 20-electron ECP are expected to lead to improvement of the results over those

obtained with the LANL2DZ basis set. The data in Figure 1 show that the results indeed improve when the Couty−Hall basis set is used instead of the Hay−Wadt basis set. This improvement was only a slight one when the MP2 and CCSD(T) methods were used, in which the deviation from the experimental $^1S \leftrightarrow {}^3P$ transition energy remained several thousand inverse centimeters. A much larger improvement resulted when the Couty−Hall basis set was used with the DFT functionals B3LYP and B3PW91, which gave deviations of only a few hundred inverse centimeters from the experimental transition energy. We note, however, that when a good agreement with experiment is obtained, this could be either due to the use of a reliable theoretical treatment or due to a fortuitous cancellation of method and basis set errors. An excellent illustration of the virtue of using correlation-consistent basis sets to unravel this issue is seen in the MP2 data in Figure 1. The $^1S \leftrightarrow {}^3P$ transition energy of the Hg atom calculated with the smallest, double-ζ, correlation-consistent basis set (cc-pRVDZ) is very close to the experimental value. However, this is fortuitous because, as one moves in the direction of larger more accurate basis sets, the resulting energies calculated become progressively higher toward a plateau that is about 3000 cm^{-1} away from the experimental weighted average. When the calculations are performed using the CCSD(T) method, which is a higher level of theory that is more reliable than MP2, the cc-pRVDZ basis set yields a $^1S \leftrightarrow {}^3P$ transition energy that is far from the experimental value, but using the larger cc-pRVTZ, cc-pRVQZ, and cc-pRV5Z basis sets yields values that converge to within only a few hundred inverse centimeters higher energy than experiment. The $^1S \rightarrow {}^3P$ excitation wavelength calculated using CCSD(T)/cc-pRV5Z is ∼236 nm, compared to ∼239 nm for the experimental weighted average. Using the correlation-consistent basis sets with MP2 and CCSD(T), therefore, has allowed us to conclude that the transition energy calculated using MP2/cc-pRVDZ is fortuitously close to the experimental value while the closeness of the results using CCSD(T) and at least a triple-ζ cc-pRV*x*Z basis set to the experimental value is because a reliable theoretical treatment was used. Figure 1 shows that using the cc-pRV*x*Z basis sets also gave accurate transition energies when the DFT hybrid functionals B3LYP and B3PW91 were used. B3PW91 yields transition energies that are somewhat closer to the experimental value than those calculated using B3LYP. The overall data in Figure 1 suggest that, as long as a cc-pRV*x*Z basis set of at least triple-ζ quality is utilized, using the CCSD(T), B3LYP, and B3PW91 methods should lead to electronic transition energies that are reliable, especially for assignment purposes. The results shown in Figure 1 with these method/basis set combinations are in much better agreement with the experimental data than those calculated previously. For example, the $^1S \leftrightarrow {}^3P$ transition energy of the Hg atom calculated by Balasubramanian et al.[49] was 44.35×10^3 cm^{-1}, or too high by ∼2500 cm^{-1}. Czuchaj et al. obtained even poorer values, which they attributed to the neglect of 5d electrons in the valence shell in their calculations.[48]

Metal−Metal Bonding in the Hg_2 Dimer and the $*Hg_2$ Excimer. The bonding in the mercury dimer is metallophilic in the ground state and covalent in many low-lying excited states. Due to spin−orbit coupling, the lowest energy absorption and emission bands for the dimer are ascribed to spin-forbidden transitions between the singlet ground state and low-lying triplet excited states. Following the Russell−Saunders notation scheme, the ground electronic state has a $^1\Sigma_g^+$ symmetry while the two lowest lying triplet excited states that are created by a transition from the $\sigma_u^*{}_{(6s)}$ antibonding HOMO to the $\pi_{u(6p)}$ and $\sigma_{g(6p)}$ bonding orbitals have $^3\Pi_g$ and $^3\Sigma_u^+$ total symmetries, respectively. Table 1 shows the results we obtained for the equilibrium distance (R_e) and binding energy (D_e) of these three states.

For the mercurophilic bonding in the $^1\Sigma_g^+$ ground state, it is noted that this bonding is accounted for using the MP2 and CCSD(T) methods regardless of the basis set used (Table 1). Because this bonding involves dispersion, DFT methods generally yield repulsive potential energy curves. It has been known for some time that care must be taken to determine whether a given density functional can properly determine dispersion forces, especially for interactions involving rare gas atoms.[67] The present work for the $^1\Sigma_g^+$ ground state of Hg_2 illustrates limitations of using DFT to describe systems bound by metallophilic bonding where dispersion interactions are also important. While several of the DFT curves do have minima for the $^1\Sigma_g^+$ ground state of Hg_2, these minima are above the dissociation limit. This indicates that the DFT representation of the dispersion forces was not sufficiently strong to overcome the steric or Pauli repulsion of the Hg atoms with each other. Clearly, such minima do not represent a chemically meaningful dispersion interaction. For the $^3\Pi_g$ and $^3\Sigma_u^+$ excited states, on the other hand, all methods, including DFT and HF (not shown), accounted for the Hg−Hg bonding because it is covalent. Aside from these expected qualitative trends, further discussion is warranted for some of the results in Table 1. First, it is noted that using the MP2 method gives rise to higher D_e energies and shorter R_e distances than the experimental values for both the ground state and the excited states studied. These errors are particularly significant for the ground state. For example, the MP2 D_e values for the cc-pRVTZ and cc-pRVQZ basis sets are more than 3 times larger than the CCSD(T) values obtained with the same basis sets. However, the MP2 errors are also significant for the excited $^3\Sigma_u^+$ and $^3\Pi_g$ states. There are two reasons for the limitations of the MP2 results: (1) MP2 is a second-order perturbation theory, and it may be necessary to include higher order perturbations to converge toward the exact results.[68] Indeed, when test calculations using a higher order perturbation theory were performed (MP3 and MP4), the D_e values dropped to nearly half the corresponding MP2 values. (2) Møller−Plesset perturbation theory assumes a single-configuration reference,[51] while multiconfiguration references are needed to properly describe the zeroth-order Hg_2 wave functions.[48,49] The CCSD(T) approach reduces a great part of these difficulties;[68] hence, both the D_e and R_e values shown in Table 2 using CCSD(T) were more accurate than those obtained with MP2. Second, while most of the DFT results gave negative D_e values, positive D_e values were obtained when the Couty−Hall basis set was used in conjunction with B3LYP and B3PW91. Third, some anomalous trends were obtained for the D_e and R_e values on going to larger basis sets in the cc-pRV*x*Z series such that the smooth convergence seen in the monomer data, see Figure 1, with these basis sets was not always seen for the dimer. We believe that basis set superposition errors (BSSEs), which were not included herein, represent a major reason for these trends. BSSE essentially arises due to an overdescription of the dimer relative to the monomer, and the impact on bond lengths and energies is most significant for lower level basis sets.[69,70]

The results in Table 1 are compared to the experimental values, when available, as well as to the previous calculations in refs 48 and 49. Although experimental values are not available for the Russell−Saunders states we have calculated, Balasubramanian et al. showed that the Russell−Saunders states $^1\Sigma_g^+$, $^3\Sigma_u^+$, and $^3\Pi_g$ considered in Table 1 represent 95%, 91%, and

TABLE 1: Equilibrium Internuclear Distances and Dissociation Energies for the $^1\Sigma_g^+$, $^3\Sigma_u^+$, and $^3\Pi_g$ States of Hg_2 Using Various Theoretical Treatments

	$^1\Sigma_g^+$		$^3\Sigma_u^+$		$^3\Pi_g$	
method/basis	R_e (Å)	D_e (cm^{-1})	R_e (Å)	D_e (cm^{-1})	R_e (Å)	D_e (cm^{-1})
MP2/LANL2DZ	3.521	768	2.847	7962	2.727	8013
MP2/Couty−Hall	3.516	936	2.732	10706	2.642	10476
MP2/cc-pRVDZ	3.496	937	2.702	8698	2.585	9993
MP2/cc-pRVTZ	3.444	808	2.669	8723	2.565	10466
MP2/cc-pRVQZ	3.379	926	2.653	9302	2.550	11049
MP2/cc-pRV5Z	3.331	1005	2.651	9633	2.546	11396
CCSD(T)/LANL2DZ	3.876	429	2.891	7402	2.779	8240
CCSD(T)/Couty−Hall	3.890	788	2.760	9919	2.677	10403
CCSD(T)/cc-pRVDZ	3.837	490	2.782	8093	2.659	9306
CCSD(T)/cc-pRVTZ	3.976	270	2.754	8032	2.643	9513
CCSD(T)/cc-pRVQZ	3.862	276	2.738	8494	2.626	9937
B3LYP/ LANL2DZ	−[a]		3.185	6373	2.898	8086
B3LYP/Couty−Hall	3.829	349	2.841	10463	2.700	10984
B3LYP/cc-pRVDZ	−	−	2.870	9390	2.700	10142
B3LYP/cc-pRVTZ	−	−	2.853	9263	2.692	10256
B3LYP/cc-pRVQZ	−	−	2.847	9327	2.686	10350
B3LYP/cc-pRV5Z	−	−	2.846	9350	2.684	10384
B3PW91/LANL2DZ	−	−	3.123	6255	2.857	7923
B3PW91/Couty−Hall	3.495	612	2.791	11133	2.664	11439
B3PW91/cc-pRVDZ	−	−	2.823	9620	2.667	10288
B3PW91/cc-pRVTZ	−	−	2.804	9507	2.656	10355
B3PW91/cc-pRVQZ	−	−	2.798	9594	2.651	10414
B3PW91/cc-pRV5Z	−	−	2.796	9632	2.649	10459
exptl[b]	− (3.63 ± 0.04)[88]	− (350 ± 20)[91]	−(2.5 ± 0.1)[88]	− (8 260 ± 200)[91]	−	−
	− (3.70)[89,88]	− (380 ± 15)[92]	− (380 ± 15)[92]	− (8100 ± 200)[93]	− (8100 ± 200)[93]	− (8100 ± 200)[93]
	− (3.66; 3.71)[90]	− (370 ± 40)[93]	− (370 ± 40)[93]	−	−	−
ref 48[b]	− (3.94)	− (296)	2.80 (2.83)	8095 (6204)	2.70 (−)	10050 (−)
ref 49[b]	− (3.84)	− (−)	− (2.90)	− (10870)	− (2.79)	− (12840)

[a] Blank entries in DFT results refer to calculations that gave repulsive curves or minima above the dissociation limit for the $^1\Sigma_g^+$ ground state. [b] Values enclosed in parentheses are experimental values and calculated values from refs 48 and 49 for the spin−orbit states X 0_g^+, D 1_u, and A 0_g^-, which correspond to the $^1\Sigma_g^+$, $^3\Sigma_u^+$, and $^3\Pi_g$ states, respectively (see Chart 3 and the text).

96% of the character of the wave functions for the spin−orbit levels X 0_g^+, D 1_u, and A 0_g^-, respectively.[49] The dominance of the Russell−Saunders coupling is also evident in the similarity between the R_e and D_e values quoted from ref 48 in Table 1 for the Russell−Saunders states versus the corresponding spin−orbit levels. As seen in Table 1, the R_e and D_e values we calculated using the CCSD(T) method and the cc-pRVQZ basis set for the ground state are in reasonable agreement with the experimental values; our results are at least as good as those in refs 48 and 49. There are other reports of calculations that also gave reasonable results for the ground state; for a discussion of those, we refer the reader to the review in ref 48. On the other hand, the excited-state calculations shown in Table 1 for the $^3\Pi_g$ and $^3\Sigma_u^+$ states are in good qualitative agreement with both the experimental values and the previous calculations in refs 48 and 49 for all the methods, including the DFT methods. We consider the results using the CCSD(T)/cc-pRVQZ combination to be the most reliable ones for all three states studied.

Phosphorescence and Absorption Bands of the Hg_2 Dimer. Figure 2 shows the results of the calculations of the phosphorescence wavelength corresponding to the $^3\Sigma_u^+ \rightarrow {}^1\Sigma_g^+$ transition in the Hg_2 dimer. Many of the trends seen in the monomer transition calculated in Figure 1 extend to the dimer transition calculated in Figure 2. The overall data in Figure 2 suggest that, as long as a cc-pRV*x*Z basis set of at least triple-ζ quality is utilized, the CCSD(T), B3LYP, and B3PW91 methods lead to calculated phosphorescence wavelengths that are within the experimental emission envelope of the well-known near-UV continuum emission of the Hg_2 dimer while MP2 leads to inaccurate results due to the limitations of MP2 described above. This is a useful result for assignment purposes, because it verifies that the 335 nm emission in the Hg vapor is a dimer emission related to the $^3\Sigma_u^+ \rightarrow {}^1\Sigma_g^+$ transition in Hg_2. However, care must be taken before quantitative conclusions are drawn from the results in Figure 2. This is because the $^3\Sigma_u^+ \rightarrow {}^1\Sigma_g^+$ Russell−Saunders transition calculated has an energy somewhat different from that of the D $1_u \rightarrow$ X 0_g^+ spin−orbit transition observed experimentally. Chart 3 shows the relationship between the two transitions in the context of the electronic states of the

CHART 3: Electronic States of the Mercury Dimer in the Presence and Absence of Spin−Orbit Coupling[a]

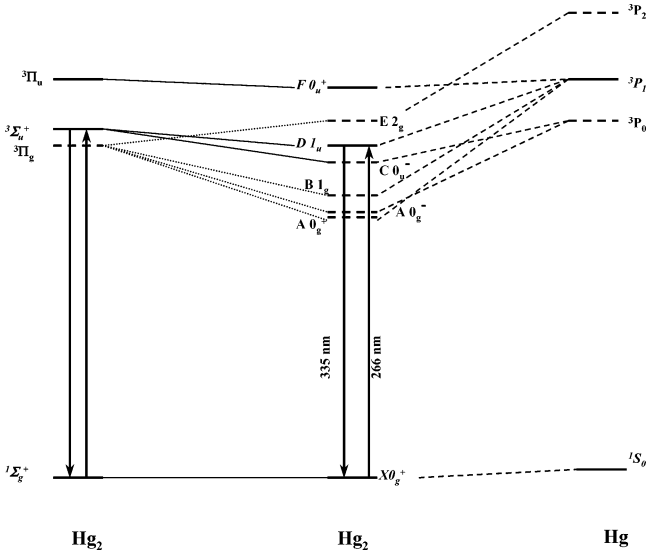

[a] Spin−orbit states involved in electric dipole allowed transitions and LS states involved in parity-allowed transitions are indicated by full lines, while the arrows represent the transitions of interest in this work. There is a slight energy difference between the $^3\Sigma_u^+$ state modeled and the D 1_u spin−orbit emitting state.

TABLE 2: Molecular Spectroscopic Parameters for the $^*Hg_2$ Excimer Using the Methods Indicated and the cc-pRVTZ Basis Set[a]

	bandwidth,[b] cm^{-1}							
method	$\nu'_{em} = 0$	$\nu'_{em} = 3$	$\nu'_{em} = 12$	SS,[c] cm^{-1}	ν'_{abs}	ω_e, cm^{-1}	$\omega_e x_e$, cm^{-1}	B_e, cm^{-1}
B3LYP	978	2308	4528	5567	40	98 (125)	0.28 (0.51)	0.021 (0.023)
B3PW91	834	2454	4530	6283	44	104 (135)	0.13 (0.68)	0.021 (0.024)
CCSD(T)	1145	3597	5534	7835	57	116 (136)	0.52 (0.90)	0.022 (0.024)
exptl[e]		2800[d]	5700[d]	7743[88,93]	57[88,93]	133;[91] 127[92] (144)[38]	0.52;[91] 0.50[92] (0.5)[38]	0.027 ± 0.002[88]

[a] Values for the nonemitting $^3\Pi_g$ state are indicated in parentheses, whereas values not in parentheses are for the emitting $^3\Sigma_u^+$ state. [b] The $\nu' = 3$ and 12 vibrational levels have Boltzmann populations of, respectively, ~50% and 10% at the experimental temperature of 763 K at which the 335 nm emission in the mercury vapor has been reported.[39] [c] SS = Stokes shift. The $^1\Sigma_g^+ \rightarrow {}^3\Sigma_u^+$ absorption energy is calculated at the experimental distance for the dimer (3.63 Å). The $^3\Sigma_u^+ \rightarrow {}^1\Sigma_g^+$ emission energy is calculated at the minimized distance of the emitting $^3\Sigma_u^+$ state for each method (see Table 1). [d] Estimated bandwidths at ~50% and 95% of the peak intensities reported in Figure 3 of ref 39. [e] Experimental values not in parentheses are for the D 1_u ($^3\Sigma_u^+$) state, while experimental values in parentheses are for the A 0_g^- ($^3\Pi_g$) state (see Chart 3 and the text).

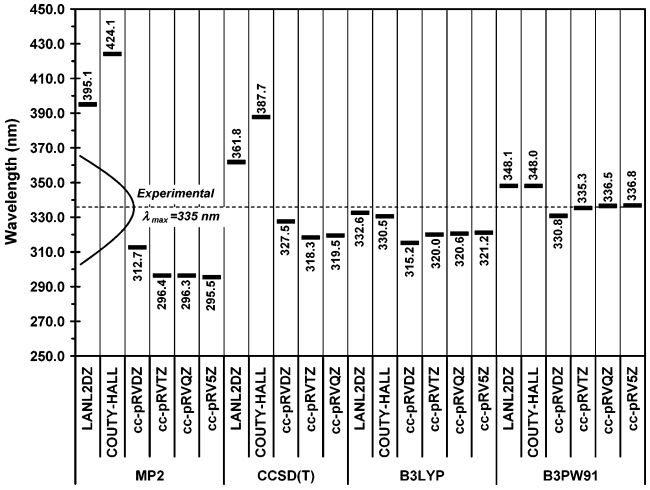

Figure 2. Calculated phosphorescence wavelength for the $^3\Sigma_u^+ \rightarrow {}^1\Sigma_g^+$ vertical transition in the Hg_2 dimer.

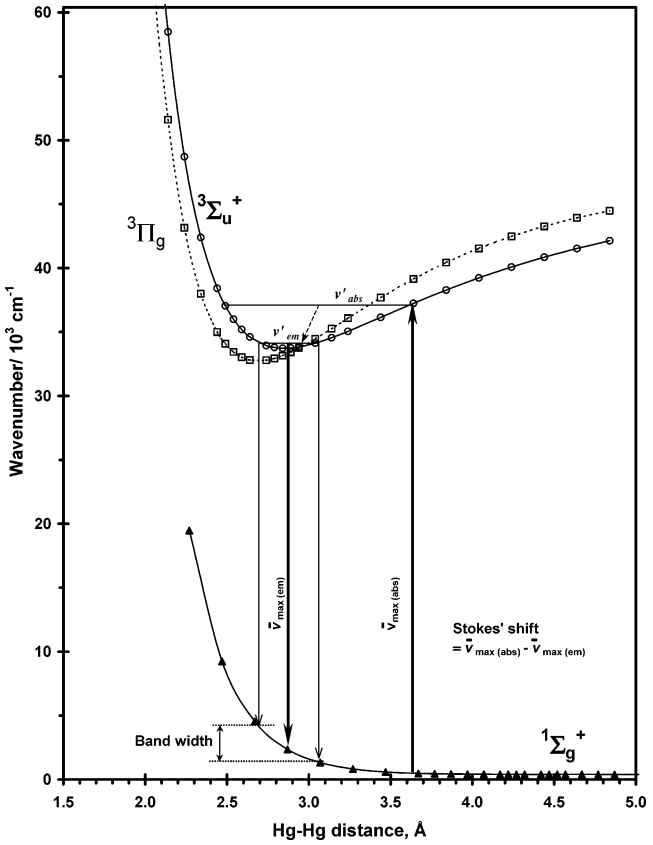

Figure 3. Potential energy surfaces for the $^1\Sigma_g^+$, $^3\Sigma_u^+$, and $^3\Pi_g$ states of Hg_2 plotted from the results of DFT calculations using the B3LYP functional and the cc-pRVTZ basis set. The figure illustrates how some spectroscopic parameters are calculated.

mercury dimer in the presence and absence of spin−orbit coupling. The excited Hg_2 $^3\Sigma_u^+$ manifold leads to D 1_u and C 0_u^- levels as a result of spin−orbit coupling. These 1_u and 0_u^- levels mix with ungerade levels with the same Ω arising from the $^3\Pi_u$ and $^1\Pi_u$ states. Because of the mixing between the D 1_u level of $^3\Sigma_u^+$ and the O 1_u level of $^1\Pi_u$, photon-induced transitions between the ground $^1\Sigma_g^+$ state and the excited $^3\Sigma_u^+$ state that are forbidden because of the $\Delta S = 0$ selection rule become electric dipole allowed.[71] While the $^3\Sigma_u^+ \rightarrow {}^1\Sigma_g^+$ Russell−Saunders transition calculated and the D $1_u \rightarrow$ X 0_g^+ spin−orbit transition are closely related, they are not identical. Nevertheless, there is only a relatively small energy difference (<1000 cm^{-1})[48,49] between the $^3\Sigma_u^+$ state modeled and the spin−orbit 1_u emitting state. Thus, we deem the calculation of the $^3\Sigma_u^+ \rightarrow {}^1\Sigma_g^+$ transition energy without treating spin−orbit coupling useful for assignment purposes.[72]

In utilizing computational methods to model luminescence spectra, it is desirable to calculate useful parameters such as the bandwidth, Stokes shift, and excited-state vibrational quantum number initially populated in the absorption transition (ν'_{abs}). These parameters quantify the extent of excited-state distortion and distinguish luminescence bands associated with a largely distorted excited state such as the case in the mercury excimer emission herein from luminescence bands associated with less distorted excited states such as monomer emissions in aromatic hydrocarbons, for example. We are unaware of any prior study for Hg_2 or any other luminescent transition-metal system in which these parameters were evaluated using modern quantum mechanical methods. For the calculation of these parameters, it is important to construct and analyze potential energy curves for the electronic ground state and emitting excited state. This is illustrated in Figure 3 for the mercury dimer, and the results of the analyses are shown in Table 2. Because the bonding is quite different in the ground and excited states of Hg_n, there is a significant Stokes shift of several thousand inverse centimeters. Another important consequence of the large shift in R_e between the ground state and the emitting excited state is a substantial broadening of the absorption and emission bands. The spatial extent of the vibrational level in the initial state leads to a Franck−Condon envelope for the transition.[73] We estimate this Franck−Condon broadening by using a simple approximation based on the vertical transition energies at the classical turning points of the initial state vibrational levels.[73,74] The calculations were based on the CCSD(T), B3LYP, and B3PW91 methods and the cc-pRVTZ basis set because these combinations have led to reasonable spectroscopic results for the Hg monomer and dimer as demonstrated above. The methodology is straightforward; however, several notes are warranted here. First, when

excited-state calculations are performed, the identity of the emitting state must be confirmed because this state is not always the lowest energy excited state.[75] As shown in Figure 3, the $^3\Sigma_u^+$ emitting state is lower in energy than the $^3\Pi_g$ nonemitting state at longer R distances but the order is switched at shorter R distances. Obviously, the absorption energy, Stokes shift, bandwidth, and ν' values should all be evaluated on the basis of the $^3\Sigma_u^+$ emitting state. Second, the bandwidth was evaluated on the basis of $\nu'_{em} = 0$, 3, and 12 for $^*Hg_2$. The calculation based on $\nu' = 0$ gives the inherent broadening of the electronic emission band at 0 K without thermal broadening; therefore, it is a fundamentally useful parameter to distinguish broad from narrow emissions. While this calculation would be useful to relate to experimental results for solid-state luminescent materials, for which measurements at cryogenic temperatures are readily obtained and will not have significant thermal population of excited vibrational levels, the $\nu' = 0$ bandwidth calculation does not have strong bearing on the Hg_2 system because the experimental data are obtained at very high temperatures (e.g., 763 K in ref 39). At such temperatures, excited vibrational levels are significantly populated. A commonly used parameter in experimental luminescence studies is the full width at half-maximum (fwhm). A reasonable estimation of fwhm for the 335 nm $^*Hg_2$ excimer emission is the bandwidth based on the $\nu' = 3$ level, which has a Boltzmann population of ~50% at 763 K. It may be more desirable to calculate the full width of the emission band instead of the more subjective fwhm. For the full-width calculation, levels that have 5−10% Boltzmann populations are assumed to contribute to the broadening beyond the noise level in the experimental spectra. Thus, we approximate the full-width calculations in Table 2 on the basis of the $\nu' = 12$ level. In the full-width calculations, we included anharmonicity because it is expected to lead to modest changes in the estimates of the band broadening. The inclusion of anharmonicity is even more important for the determination of ν'_{abs} because of the very high vibrational levels involved.

As shown in Table 2, the calculated spectroscopic results for the mercury dimer are very reasonable and in good agreement with the experimental values available. The large values of the bandwidth, Stokes shift, and ν'_{abs} shown in Table 2 are convenient probes to numerically describe the very large excited-state distortion in the $^*Hg_2$ excimer. Successful calculation of these parameters demonstrates that the use of computational methods in modeling luminescent materials should be expanded beyond merely the calculation of the emission energy and optimizing the structure of the excited molecule. The calculated vibrational and rotational parameters shown are also in very good agreement with the experimental results available (Table 2).

The limitation of DFT methods in describing dispersion forces has an important consequence on the utilization of these methods in calculating the absorption energies. A reasonable way to estimate the absorption energy with DFT methods in such cases is to calculate the vertical transition at the experimental distance (3.63 Å for Hg_2,[88] Figure 3). MP2 and CCSD(T) do not suffer this limitation, so in principle, the absorption energies may be calculated on the basis of the optimized ground-state geometries with these methods. However, because the ground state is rather shallow, there are large uncertainties in the calculation of the R_e for the ground state; thus, the approach followed in calculating the absorption energies in Figure 4 and the consequent spectroscopic parameters in Table 2 is based on vertical transitions at the experimental ground-state distance for all methods. As shown in Figure 4, the $^1\Sigma_g^+ \rightarrow {}^3\Sigma_u^+$ absorption

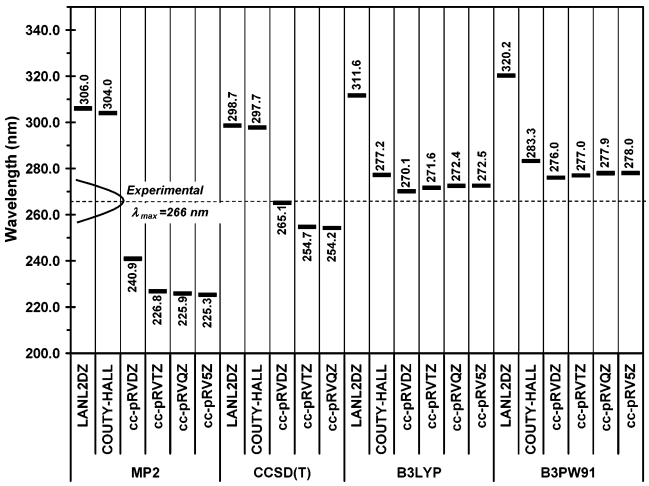

Figure 4. Calculated absorption energy for the $^1\Sigma_g^+ \rightarrow {}^3\Sigma_u^+$ vertical transition in the mercury dimer at the experimental ground-state distance of 3.63 Å.

energies calculated using this approach are reasonable when CCSD(T) and DFT methods are used in conjunction with at least a cc-pRVTZ basis set. From the data in Figure 4, the largest basis set B3LYP and B3PW91 calculations for the $^1\Sigma_g^+ \rightarrow {}^3\Sigma_u^+$ transition energy are, respectively, 900 and 1600 cm^{-1} lower in energy than the observed X $0_g^+ \rightarrow$ D 1_u absorption energy. On the other hand, the CCSD(T) absorption energy obtained using the cc-pRVQZ basis is 1700 cm^{-1} higher than the experimental absorption energy. Thus, it would appear, at first thought, that the DFT method with a B3LYP functional gives a better result for the excitation energy than does the ab initio CCSD(T) method; however, this is misleading. As we discussed above, see Chart 3, the relativistic spin−orbit corrections[48,49] for the D 1_u level are such that the transition energy between the Russell−Saunders states should be higher than the transition energy between the spin−orbit split levels.

The overall data in Figures 2−4 and Tables 1 and 2 support the literature assignment of the near-UV emission in the mercury vapor to be from the $^3\Sigma_u^+$ (D 1_u) state and provide molecular spectral parameters that quantify the large excited-state distortion. Very good agreement with the experimental data is obtained with a judicious selection of methods and basis sets. To finish the discussion of the spectroscopy of the Hg_2 dimer, we address the calculation results for the $^3\Pi_g$ state. Although this state is nonemissive because of the parity selection rule for electric dipole allowed transitions, it is a very important dimer state because it acts as a reservoir of the molecular excitation energy and, hence, is important for laser action of the mercury vapor.[37,38,48] Because this state is just lower in energy than the $^3\Sigma_u^+$ state and is a bound state with a large D_e (Table 1), it is considered a metastable state that feeds the higher energy emitting states of the dimer and trimer, as it should not decay to the ground state by an electric dipole mechanism. Nevertheless, Callear and co-workers have discovered a violet emission in the mercury vapor at ~395 nm and assigned it to a collision-induced transition from the A $0_g^{\pm}$ spin−orbit states that result from this $^3\Pi_g$ state.[38,76] Our calculations support this assignment, as broad emissions in this region were calculated for the parity-forbidden $^3\Pi_g \rightarrow {}^1\Sigma_g^+$ transition. For example, B3PW91/cc-pRV5Z calculations give rise to a phosphorescence wavelength of ~370 nm due to this transition. The $^3\Pi_g \rightarrow {}^1\Sigma_g^+$ transition energies calculated have more significant differences from the experimental results than those above for the $^3\Sigma_u^+ \rightarrow {}^1\Sigma_g^+$ transition energies calculated with the same method/basis set combinations. This is because the discrepancy between the

TABLE 3: Bonding and Molecular Spectroscopic Parameters for the *Hg_3 Linear Trimer Exciplex Using the B3PW91 Method and the cc-pRVTZ Basis Set

	$^3\Pi_u$	$^3\Sigma_u^+$		$^3\Pi_u$	$^3\Sigma_u^+$
R_e, Å	2.715[a]	2.842[a]	Stokes shift,[c] cm^{-1}	14341	8733
D_e,[b] cm^{-1}	14828	13924	ν_{abs}[c]	130	83
$\lambda_{emission}$, nm	480.0	415.4	ω_e,[e] cm^{-1}	83	69
$\lambda_{absorption}$,[c] nm	284.3	304.8	$\omega_e x_e$,[e] cm^{-1}	0.12	0.040
bandwidth, cm^{-1}; $\nu_{em} = 0$	967	920	B_e, cm^{-1}	0.0057	0.0050
bandwidth,[d] cm^{-1}; $\nu_{em} = 5$	4724	3063			
bandwidth,[d] cm^{-1}; $\nu_{em} = 18$	8538	5758			

[a] The two Hg−Hg distances were found to be identical in the optimized geometries. [b] The dissociation is to one excited (^{3}P) *Hg atom and two ground-state (^{1}S) Hg atoms. [c] The absorption wavelengths and ν'_{abs} values are calculated at 3.56 Å (see the text for an explanation of the choice of this distance). [d] The $\nu' = 5$ and 18 vibrational levels have Boltzmann populations of, respectively, ∼50% and 10% of the population of the $\nu' = 0$ level at the experimental temperature of 763 K at which the 485 nm emission in the mercury vapor has been reported.[39] [e] Symmetric stretch.

$^3\Sigma_u^+$ calculated and the near-UV emitting D 1_u state is much smaller than that between the $^3\Pi_g$ state calculated and the violet emitting A $0_g^\pm$ spin−orbit states (Chart 3). If calculations that do not include spin−orbit coupling are used to model the luminescence of heavy metal species, one has to tolerate deviations from experimental values such as those calculated here for the $^3\Pi_g \rightarrow {}^1\Sigma_g^+$ transition. For assignment purposes, however, such deviations are normally acceptable.

Bonding and Spectroscopy for the Linear Mercury Trimer. The assignment of the 485 nm emission in the mercury vapor has been subject to controversy. Initially, this band has been assigned to a collision-induced transition from a spin−orbit state of the *Hg_2 excimer that is below the D 1_u state.[40,41] However, more extensive experimental[39,42] and theoretical[43] investigations have indicated that the green emission could not be assigned to a dimer; instead, it has been assumed to originate from a phosphorescent trimer exciplex, *Hg_3.[38,44] Prior to the present work, this assignment had not been confirmed by a theoretical treatment of the trimer. Table 3 summarizes our calculations of several bonding and spectroscopic parameters for the low-lying triplet states of the linear Hg_3 trimer. The DFT results in Table 3 have been obtained using the B3PW91 functional and the cc-pRVTZ basis set. For the absorption energies to the excited states, we consider vertical transitions at the Hg−Hg bond distance of 3.56 Å; as explained below, this is our best estimate of the bond distance in the ground state of the linear Hg_3 trimer. We find that the linear $D_{\infty h}$ symmetry is preferred over the bent C_{2v} symmetry for both the ground and the lowest triplet states of the trimer. This contradicts an earlier study by Baştuğ et al., where they obtained a minimum for the ground state of the trimer that has a C_{2v} symmetry.[77] Because these authors obtained rather inaccurate energies for the monomer, dimer, and trimer using a Dirac−Fock−Slater SCF approach,[77] we believe that the linear $D_{\infty h}$ symmetry we obtained is the lower energy geometry for the ground and lowest triplet states of the Hg_3 trimer.

In the $D_{\infty h}$ linear Hg_3 trimer, a transition from the antibonding HOMO, $\sigma_g^*{}_{(6s)}$, to the two lowest lying virtual orbitals, the $\sigma_{u(6p)}$ and $\pi_{u(6p)}$ bonding MOs, leads to ungerade states. Hence, the resulting lowest triplet states, $^3\Sigma_u^+$ and $^3\Pi_u$, are both emitting states. Table 3 shows that both states are strongly bound, as evidenced by the short R_e distances and high D_e energies. The next section contains more insights regarding the bonding properties in the trimer versus smaller and larger clusters in various electronic states, including the ground state (results for the ground state are not shown in Table 3 because a DFT treatment is followed). The results in Tables 3−5 represent the first spectroscopic parameters calculated for the linear Hg_3 species, to our knowledge. The linear trimer $^3\Sigma_u^+$ and $^3\Pi_u$ states will lead to three low-lying spin−orbit states that can decay radiatively to the ground state according to Hund's case (c) selection rules, one 0_u^+ state and two 1_u states.[38] The green continuum emission at 485 nm known in the mercury vapor has been suspected to be related to the A 0_u^+ spin−orbit trimer state.[38] The calculated results in Table 3 provide the first computational support of this assignment. These results show the following: (1) The lower energy emission is from the $^3\Pi_u$ state, to which the A 0_u^+ spin−orbit trimer level correlates. (2) The emission wavelength calculated is 480 nm for the $^3\Pi_u$ state using B3PW91/cc-pRVTZ, very close to the 485 nm experimental emission attributed to the trimer. This particular B3PW91/cc-pRVTZ treatment came within only a few nanometers of the experimental values for the triplet → singlet transitions in the monomer (241 vs 239 nm) and dimer (335 vs 335 nm), so the errors associated with this method and basis set combination seem to offset the errors that arise because we have neglected spin−orbit coupling. (3) The bandwidths, Stokes shifts, and ν'_{abs} values shown in Table 3 clearly illustrate a very large excited-state distortion in the emitting state, even more so than in the *Hg_2 excimer. The bandwidths calculated at $\nu'_{em} = 5$ and 18 in Table 3 are to be compared with experimental values of 4500 and 8200 cm^{-1} that we estimated for the bandwidths at ∼50% and 95% of the peak intensities reported in Figure 4 of ref 39. There are no experimental values available yet for the Stokes shift or ν'_{abs} for the 485 nm trimer emission because this emission is usually obtained by excitations corresponding to the atomic $^1S \rightarrow {}^3P_2$ transition at ∼253 nm, which excites the Hg monomer instead of directly exciting the trimer or dimer.[38−42] It is interesting to note that Table 3 predicts that the lowest energy absorption involves excitation to the $^3\Sigma_u^+$ state while the lowest energy emission occurs from the $^3\Pi_u$ state. Consequently, the $^3\Pi_u$ emission is predicted to have a much larger excited-state distortion than the $^3\Sigma_u^+$ emission, which is translated to smaller bandwidths, Stokes shifts, and ν'_{abs} values for the $^3\Sigma_u^+$ emission. Other trimer bands besides the 485 nm emission are not very well known in the mercury vapor. However, in recent experiments on the emission in mercury vapor, Koperski et al. used a supersonic expansion beam under conditions that favor high collision rates. As a result, they have observed three continuum emissions at 404, 436, and 500 nm.[78] The latter band is the same historically known 485 nm green emission in mercury vapor; variations in experimental conditions are known to lead to some changes in the peak maxima of the various continuum bands in the mercury vapor. These three peaks were assigned to the Hg_3 trimer,[78] but the authors stated that the assignment is tentative and needs to be confirmed by mass analysis, and they did not assign the three bands to specific electronic states of a linear or bent trimer. We note that the 404 nm emission in ref 78 attributed to the trimer occurs at a wavelength very similar to that of the violet emission that Callear et al. presented strong evidence that it should be assigned to a collision-induced transition from the dimer A $0_g^\pm$ state.[38,76]

The extremely high carrier gas pressures (~10 atm) used in ref 78 should favor collision-induced bands. For these reasons, we believe that the 404 nm emission observed by Koperski et al. should be assigned to the dimer A $0_g^{\pm}$ state instead of a trimer state. This leaves the 436 nm band in ref 78 unassigned. The calculations in Table 3 are consistent with an assignment of this band to a spin−orbit state related to the $^3\Sigma_u^+$ state of the linear trimer. The energy difference between the calculated $^3\Sigma_u^+ \rightarrow {}^1\Sigma_g^+$ phosphorescence wavelength of the trimer and the 436 nm experimental emission is similar to the energy difference between the calculated $^3\Pi_u \rightarrow {}^1\Sigma_g^+$ phosphorescence wavelength of the trimer and the 500 nm experimental emission in ref 78. However, a more definitive assignment of the trimer emission bands must await further calculations we plan that treat spin−orbit coupling. We believe that these results in Table 3 will serve as a backdrop for future experimental and theoretical work on the mercury trimer because much about the spectroscopy of this species remains unknown.

Cooperativity of the Hg−Hg Bonding in Hg_n Oligomers and $^*Hg_n$ Exciplexes. An important issue in metallophilic bonding is whether there is a driving force for expanding the bonding beyond one bond in an extended system. This is an important structural issue to understand because solid-state systems that exhibit metallophilic bonding often exhibit intermolecular M−M interactions that range from dimers and larger oligomers to extended chains and sheets. Herein we address this issue of cooperativity for both the ground-state mercurophilic bonding in Hg_n oligomers and the excited-state covalent bonding in $^*Hg_n$ exciplexes. We consider linear systems with 1−4 atoms. In choosing the appropriate method and basis set combination for this study, one needs to choose a combination that describes the systems well while maintaining the feasibility of the calculations for the larger clusters. It is very critical that one chooses a method that accounts for dispersion. Hence, correlated ab initio methods such as MP2 and CCSD(T) work well for this study, while HF and various DFT functionals do not. In this connection, it is appropriate to consider how well MP2 describes the van der Waals dispersion interaction; this is particularly important for our analysis of the ground states of the Hg_n oligomers. For this purpose, we review the results that Burda et al. have obtained in a detailed and careful study of the D_e and R_e for rare gas dimers.[79] Since these dimers are bound purely by dispersion forces, the comparison by Burda et al.[79] of the accuracy of MP2 and CCSD(T) treatments is quite relevant for the bonding in the ground states of the Hg_n systems. It was found that, while the CCSD(T) D_e values are reasonably close to results obtained with still more accurate methods, the MP2 D_e values have significantly larger errors.[79] The MP2 D_e values are 15−35% different from the CCSD(T) values. Moreover, the MP2 D_e values are sometimes smaller and sometimes larger than the reasonably accurate CCSD(T) values; for He_2 and for Ne_2, the MP2 D_e values are too small, while for Ar_2, Kr_2, and Xe_2, the MP2 D_e values are too large. The MP2 D_e values being too large for heavy dimers is consistent with our results for the $^1\Sigma^+$ ground state of Hg_2, see Table 1, where the MP2 D_e value is too large by 0.08 eV compared to the CCSD(T) value. For the R_e, Burda et al. find that the MP2 values are close to the CCSD(T) values, differing from them by only ~2−3%.[79] These smaller MP2 errors for R_e are also reflected in our results for Hg_2. The basis set choice is also important; however, all basis sets discussed above are reasonable when coupled with the proper method. Hence, we have chosen the MP2/LANL2DZ combination in this study of cooperativity. An inspection of Table 1 above for the dimer reveals that this combination describes the ground-state mercurophilic bonding (with a positive D_e), correctly predicts that the bonding increases by an order of magnitude in the triplet excited states studied, and that the bonding is stronger in the $^3\Pi_g$ state than in the $^3\Sigma_u^+$ state. This validates the MP2/LANL2DZ combination for the study of cooperativity. This conclusion is strongly supported by the comparisons made by Burda et al. for the D_e and R_e of rare gas dimers between MP2 and CCSD(T).[79]

TABLE 4: Ground-State Cooperativity in Hg_n Linear ($D_{\infty h}$) Oligomers According to MP2/LANL2DZ Calculations

"n" in Hg_n	R_e, Å	E/n, cm^{-1}	D_e, cm^{-1}	D_e/bond, cm^{-1}
2	3.521	−384	768	768
3	3.450, 3.450	−613	1838	919
4	3.419, 3.389, 3.419	−756	3025	1008

Table 4 shows the calculated equilibrium distances, the binding energies per atom (E/n), the total binding energies for dissociation to separated atoms (D_e), and the binding energies per bond (D_e/bond) for the ground states of linear Hg_n oligomers ($n = 2$, 3, and 4). For the binding energies, the energy of the ^1S ground state of the Hg atom is the reference energy. The data show an unmistakable trend that the mercurophilic bonding in the electronic ground state is cooperative. As one moves toward larger clusters, the internuclear distances become shorter, and the total and average binding energies become higher. If one accepts the premise that the mercurophilic bonding in the Hg_n system is a good model for the general metallophilic bonding in closed-shell transition-metal complexes, this trend will then explain the experimental finding that these complexes have a strong tendency to form supramolecular assemblies in the form of oligomers and extended structures with M−M interactions.[5] Previous studies by Omary and Patterson suggested, on the basis of extended Hückel calculations, that the argentophilic and aurophilic bonding in $[Ag(CN)_2^-]_n$ and $[Au(CN)_2^-]_n$ oligomers, respectively, is also cooperative.[80] In the mercury system itself, the ground-state cooperativity in the Hg−Hg bonding per the results in Table 4 is consistent with the experimental fact that cooling mercury vapor after supersonic expansion experiments has often led to the formation of large clusters instead of just dimers or trimers.[81] Furthermore, informed prediction of the geometry of Hg_n species that have yet to be characterized can be made on the basis of these results. For example, the internuclear distances in the linear Hg_3 trimer have yet to be characterized experimentally. Since the calculations in Table 4 predict a shortening by ~0.07 Å on going from the dimer to the trimer, combining this finding with the experimental distance in the dimer leads to a prediction that the linear Hg_3 trimer will have two identical distances of ~3.56 Å.

To analyze the bonding in the excited states, we first discuss the orbital nature of the excitations considered for Hg_4; the orbital nature of the excitations in Hg_2 and Hg_3 has been discussed earlier. The HOMO of Hg_4 is the 6s σ_u^* orbital that is antibonding between all Hg atoms; see Figure 5. For the triplet excited states of Hg_4, we consider states created by spin-forbidden transitions from this HOMO to bonding 6p σ_g and π_u orbitals to form $^3\Sigma_u^+$ and $^3\Pi_g$ states, respectively. The second-highest occupied Hg_4 orbital is a 6s σ_g, which is bonding between the central Hg pair of atoms but antibonding between the outer two pairs of Hg atoms. We consider high-spin excited states where the total state is a coupled quintet. The two quintets that can be formed are $^5\Pi_g$ and $^5\Sigma_u^-$. The issue of excited-state cooperativity is harder to assess than the cooperativity in the ground state. This is because excited-state bonds differ in

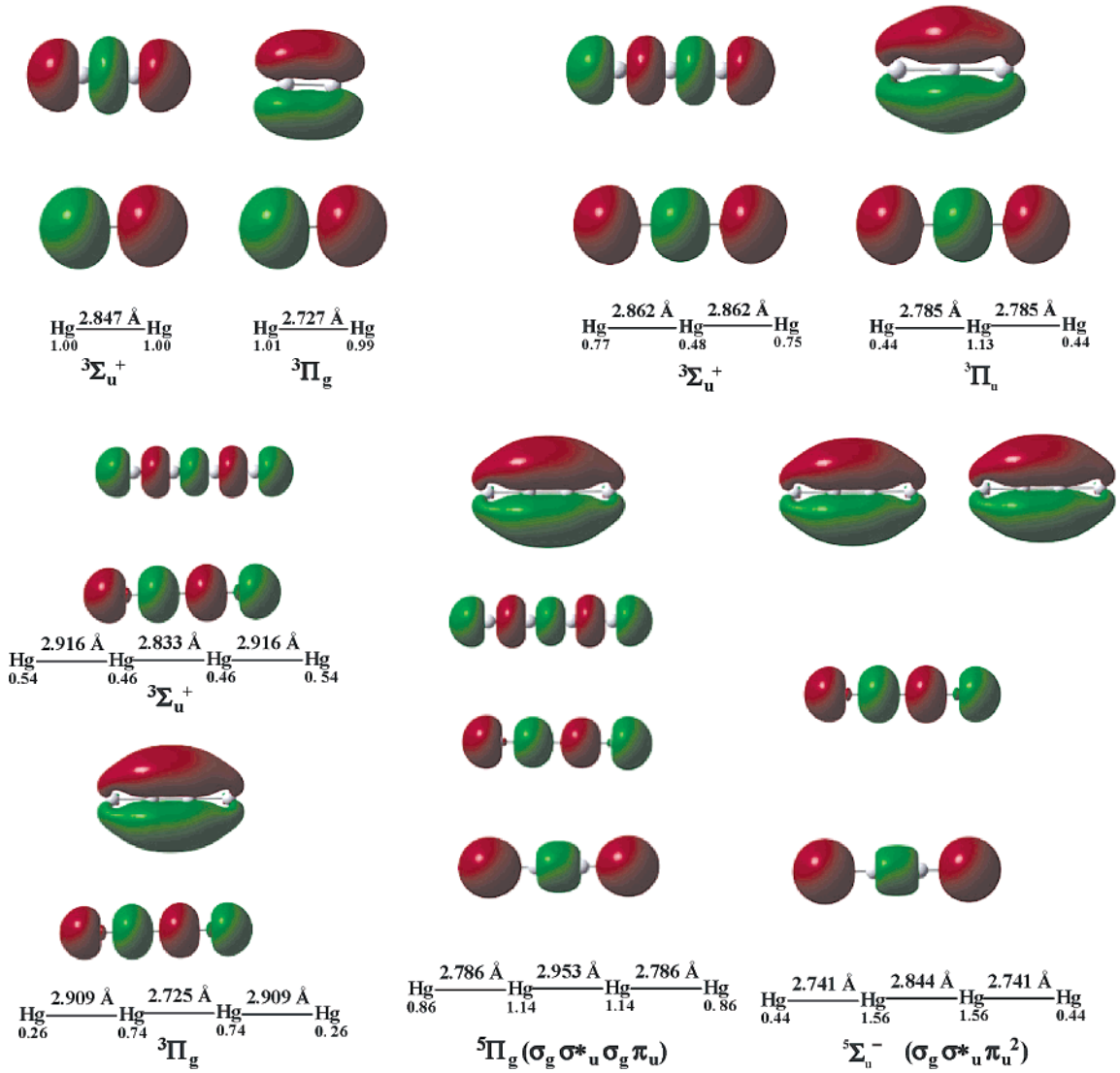

Figure 5. Equilibrium distances, spin densities, and contours of the SOMOs for the low-lying paramagnetic states of linear Hg_n oligomers ($n = 2-4$).

strength in different oligomers in the absence of cooperativity while in the ground-state all oligomers have a formal bond order of 0. A one-photon excitation from an antibonding to a bonding orbital to form a triplet excited state, for example, involves an increase in the formal bond order from 0 in all oligomers to 1 in a dimer (one bond), 1/2 in a trimer (two bonds), and 1/3 in a tetramer (three bonds) in the absence of cooperativity. Therefore, the basis in evaluating the cooperativity in the excited state will be the total stabilization energy for all bonds in the oligomers, as opposed to individual bond lengths and energies. The results for low-lying paramagnetic states of $*Hg_n$ ($n = 1-4$) linear exciplexes are shown in Table 5, and their geometries and spin densities are shown in Figure 5. The cooperativity in the Hg−Hg bonding is clearly illustrated in the Table 5 entries. As one moves toward larger clusters in either $^3\Sigma$ or $^3\Pi$ states, the binding energy per atom and the average bond energy both become higher. This occurs despite the fact that the individual bonds may be weaker, on average, as one moves in this direction (see the bond lengths in Figure 5). The increased stabilization on going to longer oligomer exciplexes is several thousand inverse centimeters per atom added, compared to only a few hundred inverse centimeter increases seen in Table 4 for the ground-state oligomers, although the total formal bond order expected without cooperativity is uniform in each case (0 for the ground states and 1 for the triplet states). This suggests that the excited-state cooperativity is stronger than the ground-state cooperativity. Another very important result in Table 5 is that lower energies and higher binding energies are obtained for the quintet tetramers compared to two separated triplet dimers. This means that the energy of two excited dimers that ferromagnetically couple with one another to form a quintet is lower than

TABLE 5: Excited-State Cooperativity in $*Hg_n$ Linear Oligomer Exciplexes According to MP2/LANL2DZ Calculations

"n" in $*Hg_n$	state	E/n,[a] 10^3 cm^{-1}	D_e,[b] 10^3 cm^{-1}
2	$^3\Sigma_u^+ (\sigma_u^*{}_{(6s)}\sigma_{g(6p)})$	−21.16	7.962
3	$^3\Sigma_u^+ (\sigma_g^*{}_{(6s)}\sigma_{u(6p)})$	−27.17	12.80
4	$^3\Sigma_u^+ (\sigma_u^*{}_{(6s)}\sigma_{g(6p)})$	−29.68	15.67
2	$^3\Pi_g (\sigma_u^*{}_{(6s)}\pi_{u(6p)})$	−21.19	8.013
3	$^3\Pi_u (\sigma_g^*{}_{(6s)}\pi_{u(6p)})$	−27.10	12.57
4	$^3\Pi_g (\sigma_u^*{}_{(6s)}\pi_{u(6p)})$	−29.63	15.46
4	$^5\Pi_g (\sigma_{g(6s)}\sigma_u^*{}_{(6s)}\sigma_{g(6p)}\pi_{u(6p)})$	−22.70	22.07
4	$^5\Sigma_u^- (\sigma_{g(6s)}\sigma_u^*{}_{(6s)}\pi_{u(6p)}\pi_{u(6p)})$	−22.12	19.77

[a] Relative to the energy of a *Hg atom in the ^{3}P state. [b] D_e values were calculated for $*Hg_n$ exciplexes such that triplet states dissociate to one ^{3}P *Hg atom and "n − 1" ^{1}S ground-state Hg atoms while the quintet tetramers dissociate to two ^{3}P *Hg atoms and two ^{1}S Hg atoms.

the energy of two isolated triplet dimers. This suggests that solid-state linear-chain materials systems that exhibit excited-state cooperativity and excimer/exciplex-forming properties similar to those of the mercury system may stabilize high-spin excited states. This would be extremely significant if proved experimentally because such materials would be ideal as magnetic switching devices, which have been receiving significant interest lately.[33] The magnetic behavior would be "turned on" by light exposure, while it turns off in the dark because the material is diamagnetic in the ground state. Further treatment of linear and nonlinear clusters of group 12 elements, including larger clusters and different spin states, is in progress.

The cooperative bonding in linear mercury clusters should be viewed as long-range/multicenter bonding, as opposed to the classical two-electron/two-center covalent bonding. An inspection of Figure 5 supports this conclusion because it shows that (1) all bonds in $^*Hg_n$ exciplexes are shortened rather significantly from the ~3.5 Å ground-state distances, (2) the electron densities in the bonding orbitals span all atoms in the cluster, and (3) the spin densities are delocalized onto all atoms. While the extent of each of these trends varies depending on the oligomer size and the state, a general delocalization of the bonding and paramagnetism is evident from the data shown in Figure 5. The cooperativity of the excited-state bonding in $^*Hg_n$ exciplexes deduced from Table 5 and Figure 5 also explains several aspects of the luminescence behavior of the mercury vapor and related materials that exhibit excimer/exciplex emissions. First, although the 485 nm green emission is the most well-known visible emission, it is not the lowest energy emission reported thus far in the mercury vapor. For example, lower energy emissions were reported,[82] and further experimental research under high pressure is needed, as suggested by the study in ref 78, which may lead to further lower energy visible or near-IR bands from large $^*Hg_n$ clusters. Second, the finding that the cooperativity effect is stronger in the excited state than in the ground state explains the larger Stokes shift and much lower emission energies for the larger clusters. This is evident from both the calculated spectral parameters for the dimer vs trimer in Tables 2 vs 3, respectively, and the experimental findings for both the mercury vapor and other related systems. For example, a variety of two-coordinate d^{10} complexes that pack as linear chains with M−M interactions have been reported to exhibit emissions in the red region, while they are white and absorb only in the UV region at very short wavelengths![23,24,83] A recent study by Omary et al. has shown that RNCAuX complexes that pack as linear chains have much lower emission energies and much larger apparent Stokes shifts than those in analogous dimeric materials of the same class.[84]

Concluding Remarks

This study demonstrates effective use of different theoretical treatments and approximations to prescribe methods and basis set combinations that are suitable to solve specific spectroscopic and bonding problems. We have shown that informed assignments of electronic transitions have been made for the Hg_n clusters based on the energies, bandwidths, and other spectroscopic parameters that were in good agreement with the experimental parameters available. The variations in the experimental data are usually large enough to be comparable to errors due to the neglect of spin−orbit coupling in an otherwise rigorous treatment of heavy metal systems. In the Hg vapor system, for example, the emission maxima have been reported anywhere between ~475 and 500 nm for the trimer and between 325 and 350 nm for the dimer due to changes in temperature, carrier gas, pressure, equipment setup, and other experimental factors. Hence, calculations that predict the energy range and estimate spectroscopic parameters that characterize the excited-state distortion are invaluable for such situations as this study demonstrates. Accurate calculations of the theoretical spectral and bonding parameters will require full relativistic treatment of spin−orbit effects using relativistic, four-component spinor, Dirac−Fock−CI wave functions and are extremely demanding. While we plan to pursue such calculations for the small mercury clusters, the current state-of-the-art of computational resources does not allow a similar treatment of large clusters or realistic models for large ligand-containing transition-metal complexes for which the Hg_n system is a good model. Calculations that qualitatively characterize the bonding in Hg_n linear clusters have demonstrated the significance of cooperativity in both the weakly bound ground state and strongly bound low-lying paramagnetic excited states. These results carry significance for extended-chain solid-state systems that may be helpful for the utilization and design of luminescent and magnetic materials that have bonding and spectroscopic behavior similar to that of the Hg_n system. Our efforts will continue to study larger Hg_n clusters with different geometries as well as phosphorescent closed-shell transition-metal complexes in coordination with the evolving experimental studies. This is an era where experimental methods that directly probe the excited-state structure by time-resolved methods of diffraction (photocrystallography),[85] EXAFS,[86] and Raman spectroscopy[87] are available. To make maximum use of the information gained from these elegant methods, it will be extremely important to increase the utilization of computational methods to study the excited states of luminescent organic and inorganic materials of current interest.

Acknowledgment. We acknowledge partial support of this work by the Robert A. Welch Foundation (Grant B-1542 to M.A.O.) and equipment support by the National Science Foundation (Grant CHE-0342824 to A.K.W. and P.S.B.). Computer resources were, in part, provided by the National Computational Science Alliance under Grant Nos. CHE010021 (A.K.W.) and CHE030046 (P.S.B.) and utilized the NCSA SGI Origin 2000 and IBM p690. Additional computational support was provided by the Academic Computing Services at the University of North Texas on the UNT Research Cluster. We also thank Professor Kirk Peterson for kindly providing the cc-pRV*x*Z basis sets.

References and Notes

(1) Barakat, K. A.; Cundari, T. R.; Omary, M. A. *J. Am. Chem. Soc.* **2003**, *125*, *42*, 14228.

(2) Zhang, H.-X.; Che, C.-M. *Chem.—Eur. J.* **2001**, *7*, 4887.

(3) Fernandez, E. J.; Gimeno, M. C.; Laguna, A.; Lopez-de-Luzuriaga, J. M.; Monge, M.; Pyykkö, P.; Sundholm, D. *J. Am. Chem. Soc.* **2000**, *122*, 7287.

(4) Makedonas, C.; Mitsopoulou, C. A.; Lahoz, F. J.; Balana, A. I. *Inorg. Chem.* **2003**, 42, 8853.

(5) For a review, see: Pyykkö, P. *Chem. Rev.* **1997**, *97*, 599.

(6) (a) Merz, K. M., Jr.; Hoffmann, R. *Inorg. Chem.* **1988**, *27*, 2120. (b) Jiang, Y.; Alvarez, S.; Hoffmann, R. *Inorg. Chem.* **1985**, *24*, 749. (c) Mehrotra, P. K.; Hoffmann, R. *Inorg. Chem.* **1978**, *17*, 2187. (d) Dedieu, A.; Hoffmann, R. *J. Am. Chem. Soc.* **1978**, *100*, 2074.

(7) (a) Schmidbaur, H. *Gold Bull.* **1990**, *23*, 11. (b) Schmidbaur, H. *Chem. Soc. Rev.* **1995**, 391. (c) Grohmann, A.; Schmidbaur, H. In *Comprehensive Organometallic Chemistry II*; Abel, E. W., Stone, F. G. A., Wilkinson, G., Eds.; Pergamon: Oxford, 1995; Vol. 3, Chapter 1.

(8) Pyykkö, P.; Li, J.; Runeberg, N. *Chem. Phys. Lett.* **1994**, *218*, 133.

(9) (a) Omary, M. A.; Webb, T. R.; Assefa, Z.; Shankle, G. E.; Patterson, H. H. *Inorg. Chem.* **1998**, *37*, 1380. (b) Singh, K.; Long, J. R.; Stavropoulos, P. *J. Am. Chem. Soc.* **1997**, *119*, 2942.

(10) Rawashdeh-Omary, M. A.; Omary, M. A.; Fackler, J. P., Jr. *Inorg. Chim. Acta* **2002**, *334*, 376.

(11) (a) Clodfelter, S. A.; Doede, T. M.; Brennan, B. A.; Nagle, J. K.; Bender, D. P.; Turner, W. A.; LaPunzia, P. M. *J. Am. Chem. Soc.* **1994**, *116*, 11379. (b) Nagle, J. K.; Brennan, B. A. *J. Am. Chem. Soc.* **1988**, *110*, 5931.

(12) Pettijohn, C. N.; Jochnowitz, E. B.; Chuong, B.; Nagle, J. K.; Vogler, A. *Coord. Chem. Rev.* **1998**, *171*, 85.

(13) Nagle, J. K. *Spectrum* **1999**, *12*, 15.

(14) (a) Omary, M. A.; Patterson, H. H. *J. Am. Chem. Soc.* **1998**, *120*, 7696. (b) Omary, M. A.; Patterson, H. H. *Inorg. Chem.* **1998**, *37*, 1060. (c) Omary, M. A.; Hall, D. R.; Shankle, G. E.; Siemiarczuck, A.; Patterson, H. H. *J. Phys. Chem. B* **1999**, *103*, 3845.

(15) (a) Rawashdeh-Omary, M. A.; Omary, M. A.; Shankle, G. E.; Patterson, H. H. *J. Phys. Chem. B.* **2000**, 104, 6143. (b) Patterson, H. H.; Kanan, S. M.; Omary, M. A. *Coord. Chem. Rev.* **2000**, *208*, 227.

(16) Rawashdeh-Omary, M. A.; Omary, M. A.; Patterson, H. H.; Fackler, J. P., Jr. *J. Am. Chem. Soc.* **2001**, *123*, 11237.

(17) (a) Fischer, P.; Lucas, B.; Omary, M. A.; Larochelle, C. L.; Patterson, H. H. *J. Solid State Chem.* **2002**, *168*, 267. (b) Hettiarachchi, S. R.; Rawashdeh-Omary, M. A.; Kanan, S. M.; Omary, M. A.; Patterson, H. H.; Tripp, C. P. *J. Phys. Chem. B* **2002**, *106*, 10058.

(18) Hollingsworth, G.; Barrie, J. D.; Dunn, B.; Zink, J. I. *J. Am. Chem. Soc.* **1988**, *110*, 6569.

(19) (a) Barrie, J. D.; Dunn, B.; Zink, J. I. *J. Am. Chem. Soc.* **1990**, *112*, 5701. (b) Barrie, J. D.; Dunn, B.; Holilingsworth, G.; Zink, J. I. *J. Phys. Chem.* **1989**, *93*, 3958.

(20) Mrozowski, S. *Z. Phys.* **1937**, *106*, 458.

(21) (a) Celestino, K. C.; Ermler, W. C. *J. Chem. Phys.* **1984**, *81*, 1872. (b) Houtermans, F. G. *Helv. Phys. Acta* **1960**, *33*, 933.

(22) (a) Omary, M. A.; Kassab, R. M.; Haneline, M. R.; Elbjeirami, O.; Gabbaï F. P. *Inorg. Chem.* **2003**, *42*, 2176. (b) Haneline, M. R.; Tsunoda, M.; Gabbaï F. P. *J. Am. Chem. Soc.* **2002**, *124*, 3737.

(23) Dias, H. V. R.; Diyabalanage, H. V. K.; Rawashdeh-Omary, M. A.; Franzman, M. A.; Omary, M. A. *J. Am. Chem. Soc.* **2003**, *125*, 12072.

(24) White-Morris, R. L.; Olmstead, M. M.; Balch, A. L.; Elbjeirami, O.; Omary, M. A. *Inorg. Chem.* **2003**, *42*, 6741.

(25) For reviews, see: (a) Yam, V. W.-W.; Lo, K. K. *Chem. Soc. Rev.* **1999**, *28*, 323. (b) Yam, V. W.-W.; Lo, K. K. *Mol. Supramol. Photochem.* **1999**, *4*, 31. (c) Forward, J. M.; Fackler, J. P., Jr.; Assefa, Z. Photophysical and Photochemical Properties of Gold(I) Complexes. In *Optoelectronic Properties of Inorganic Compounds*; Roundhill, D. M., Fackler, J. P., Jr., Eds.; Plenum: New York, 1999; Chapter 6.

(26) For a review, see: Sibley, S.; Thompson, M. E.; Burrows, P. E.; Forrest, S. R. Electroluminescence in Molecular Materials. In *Optoelectronic Properties of Inorganic Compounds*; Roundhill, D. M., Fackler, J. P., Jr., Eds.; Plenum: New York, 1999; Chapter 5.

(27) For a review, see: Gray, G. M.; Lawson, C. M. Structure-Property Relationships in Transition Metal-Organic Third-Order Nonlinear Optical Materials. In *Optoelectronic Properties of Inorganic Compounds*; Roundhill, D. M., Fackler, J. P., Jr., Eds.; Plenum: New York, 1999; Chapter 1.

(28) (a) Exstrom, C. L.; Sowa, J. R., Jr.; Daws, C. A.; Janzen, D.; Mann, K. R. *Chem. Mater.* **1995**, *7*, 15. (b) Daws, C. A.; Exstrom, C. L.; Sowa, J. R., Jr.; Mann, K. R. *Chem. Mater.* **1997**, *9*, 363. (c) Mansour, M. A.; Connick, W. B.; Lachicotte, R. J.; Gysling, H. J.; Eisenberg, R. *J. Am. Chem. Soc.* **1998**, *120*, 1329.

(29) For a review, see: Kalyanasundaram, K.; Grätzel, M. Efficient Photovoltaic Solar Cells Based on Dye Sensitization of Nanocrystalline Oxide Films. In *Optoelectronic Properties of Inorganic Compounds*; Roundhill, D. M., Fackler, J. P., Jr., Eds.; Plenum Press: New York, 1999; Chapter 5.

(30) (a) Kanan, S. M.; Omary, M. A.; Patterson, H. H.; Matsuoka, M. Anpo, M. *J. Phys. Chem. B* **2000**, *104*, 3507. (b) Centi, G.; Perathoner, S.; Shioya, Y.; Anpo, M. *Res. Chem. Intermed.* **1992**, *17*, 125 and references therein.

(31) (a) Horrocks, W. DeW, Jr.; Sundic, D. R. *Acc. Chem. Res.* **1981**, *14*, 384. (b) Richardson, F. S. *Chem. Rev.* **1982**, *82*, 541. (c) Horrocks, W. DeW, Jr.; Albin, M. *Prog. Inorg. Chem.* **1984**, *31*, 1.

(32) (a) Hebbink, G. A.; Reinhoudt, D. N.; van Veggel, F. C. J. M. *Eur. J. Org. Chem.* **2001**, 4101. (b) Piszczek, G.; Gryczynski, I.; Maliwal, B. P.; Lakowicz, J. R. *J. Fluoresc.* **2002**, *12*, 15.

(33) (a) Sato, O.; Iyoda, T.; Fujishima, A.; Hashimoto, K. *Science* **1996**, *272*, 704. (b) Shimamoto, N.; Ohkoshi, S.; Sato, O.; Hashimoto, K. *Inorg. Chem.* **2002**, *41*, 678.

(34) Hettiarachchi, S. R.; Patterson, H. H.; Omary, M. A. *J. Phys. Chem. B* **2003**, *107*, 14249.

(35) Dabbousi, B. O.; Rodriguez-Viejo, J.; Mikulec, F. V.; Heine, J. R.; Mattoussi, H.; Ober, R.; Jensen, K. F.; Bawendi, M. G. *J. Phys. Chem. B* **1997**, *101*, 9463.

(36) (a) Celestino, K. C.; Ermler, W. C. *J. Chem. Phys.* **1984**, *81*, 1872. (b) Houtermans, F. G. *Helv. Phys. Acta* **1960**, *33*, 933.

(37) Cefalas, A. C.; Skordoulis, C. Nicolaides, C. A. *Opt. Commun.* **1986**, *60*, 49.

(38) For reviews, see: (a) Callear, A. B. *Chem. Rev.* **1987**, *87*, 335. (b) Morse, M. D. *Chem. Rev.* **1986**, *86*, 1049.

(39) Drullinger, R. E.; Hessel, M. M.; Smith, E. W. *J. Chem. Phys.* **1977**, *66*, 5656 and references therein.

(40) Mrozowski, S. *Z. Phys.* **1937**, *106*, 458.

(41) McCoubrey, A. O. *Phys. Rev.* **1954**, *93*, 1249.

(42) (a) Callear, B. A.; Lai, K. L. *Chem. Phys.* **1982,** *69*, 1. (b) Niefer, R. J.; Supronowicz, J. B.; Atkinson, J. B.; Krause, L. *Phys. Rev. A* **1986**, *34*, 2483.

(43) (a) Mies, F. H.; Stevens, W. J.; Krauss, M. *J. Mol. Spectrosc.* **1978**, *72*, 303. (b) Smith, E. W.; Drullinger, R. E.; Hessel, M. M.; Cooper, J. *J. Chem. Phys.* **1977**, *66*, 5667.

(44) Two notes about the terminology we are adopting here versus more common terminologies used in the literature. First, an *excimer* is a homoatomic *exci*ted-state di*mer* while an *exciplex* is a more generic term that refers to an *exci*ted-state com*plex*, which could be a heteroatomic dimer (*AB), as first historically noted, $*A_{n>2}$, or $*A_nB_m$ species. The $*Hg_3$ species is not a dimer, so we prefer to refer to it as a trimer exciplex although it has been called an excimer in the literature. Second, "phosphorescence" refers to formally spin-forbidden radiative transitions such as triplet → singlet emissions. Nevertheless, phosphorescent emissions in the mercury vapor such as the 335 and 485 nm emissions have been almost invariably referred to as "fluorescence" in the literature.

(45) Munro, L. J.; Johnson, K. J.; Jordan, K. D. *J. Chem. Phys.* **2001**, *114*, 5545 and references therein.

(46) (a) Flad, H.-J.; Dolg, M. *J. Phys. Chem.* **1996**, *100*, 6147. (b) Flad, H.-J.; Dolg, M. *J. Phys. Chem.* **1996**, *100*, 6152. (c) Wang, Y.; Flad, H.-J.; Dolg, M. *Phys. Rev. B* **2000**, *61*, 2362. (d) Wang, Y.; Flad, H.-J.; Dolg, M. *Int. J. Mass Spectrom.* **2000**, *201*, 197. (e) Hartke, B.; Flad, H.-J.; Dolg, M. *Phys. Chem. Chem. Phys.* **2001**, *3*, 5121.

(47) (a) Schwerdtfeger, P.; Wesendrup, R.; Moyano, G. E.; Sadlej, A. J.; Greif, J.; Hensel, F. *J. Chem. Phys.* **2001**, *115*, 7401. (b) Moyano, G. E.; Wesendrup, R.; Söhnel, T.; Schwerdtfeger, P. *Phys. Rev. Lett.* **2002**, *89*, 103401.

(48) Czuchaj, E.; Rebentrost, F.; Stoll, H.; Preuss, H. *Chem. Phys.* **1997**, *214*, 277.

(49) Balasubramanian, K.; Das, K. K.; Liao, D. W. *Chem. Phys. Lett.* **1992**, *195*, 487.

(50) (a) Cizek, J. *Adv. Chem. Phys.* **1969**, *14*, 35. (b) Purvis, G. D.; Bartlett, R. J. *J. Chem. Phys.* **1982**, *76*, 1910.

(51) (a) Pople, J. A.; Binkley, J. S.; Seeger, R. *Int. J. Quantum Chem. Symp.* **1976**, *10*, 1. (b) Møller, C.; Plesset, M. S. *Phys. Rev.* **1934**, *46*, 618. (c) Tozer, D. J.; Andrews, J. S.; Amos, R. D.; Handy, N. C. *Chem. Phys. Lett.* **1992**, *199*, 229.

(52) Parr, R. G.; Yang, W. *Density-functional Theory of Atoms and Molecules*; Oxford University Press: Oxford, 1989.

(53) (a) Becke, A. D. *J. Chem. Phys.* **1993**, *98*, 5648. (b) Burke, K.; Perdew, J. P.; Wang, Y. In *Electronic Density Functional Theory: Recent Progress and New Directions*; Dobson, J. F., Vignale, G., Das, M. P., Eds.; Plenum: New York, 1998.

(54) See, for example: (a) Lee, Y. S.; Ermler, W. C.; Pitzer, K. S. *J. Chem. Phys.* **1977**, *67*, 5861. (b) Chrisansen, P. A.; Lee, Y. S.; Pitzer, K. S. *J. Chem. Phys.* **1979**, *71*, 4445.

(55) Frisch, M. J.; Trucks, G. W.; Schlegel, H. B.; Scuseria, G. E.; Robb, M. A.; Cheeseman, J. R.; Zakrzewski, V. G.; Montgomery, J. A.; Stratmann, R. E.; Burant, J. C.; Dapprich, S.; Millam, J. M.; Daniels, A. D.; Kudin, K. N.; Strain, M. C.; Farkas, O.; Tomasi, J.; Barone, V.; Cossi, M.; Cammi, R.; Mennucci, B.; Pomelli, C.; Adamo, C.; Clifford, S.; Ochterski, J.; Petersson, G. A.; Ayala, P. Y.; Cui, Q.; Morokuma, K.; Malick, D. K.; Rabuck, A. D.; Raghavachari, K.; Foresman, J. B.; Cioslowski, J.; Ortiz, J. V.; Stefanov, B. B.; Liu, G.; Liashenko, A.; Piskorz, P.; Komaromi, I.; Gomperts, R.; Martin, R. L.; Fox, D. J.; Keith, T.; Al-Laham, M. A.; Peng, C. Y.; Nanayakkara, A.; Gonzalez, C.; Challacombe, M.; Gill, P. M. W.; Johnson B. G.; Chen, W.; Wong, M. W.; Andres, J. L.; Head-Gordon, M.; Replogle, E. S.; Pople, J. A. *Gaussian 98*, Revision A.1; Gaussian Inc.: Pittsburgh, PA, 2001.

(56) Hay, P. J.; Wadt, W. R. *J. Chem. Phys.* **1985**, *82*, 270.

(57) Couty, M.; Hall, M. B. *J. Comput. Chem.* **1996**, *17*, 1359.

(58) (a) Fernandez-Pacios, L.; Christiansen, P. A. *J. Chem. Phys.* **1985**, *82*, 2664. (b) Hurley, M. M.; Fernandez-Pacios, L.; Christiansen, P. A.; Ross, R. B.; Ermler, W. C. *J. Chem. Phys.* **1986**, *84*, 6840. (c) LaJohn, L. A.; Christiansen, P. A.; Ross, R. B.; Atashroo, T.; Ermler, W. C. *J. Chem. Phys.* **1987**, *87*, 2812. (d) Ross, R. B.; Powers, J. M.; Atashroo, T.; Ermler, W. C.; LaJohn, L. A.; Christiansen, P. A. *J. Chem. Phys.* **1990**, *93*, 6654. (e) Ross, R. B.; Gayen, S.; Ermler, W. C. *J. Chem. Phys.* **1994**, *100*, 8145. (f) Ermler, W. C.; Ross, R. B.; Christiansen, P. A. *Int. J. Quantum Chem.* **1991**, *40*, 829.

(59) Bagus, P. S.; Bauschlicher, C. W., Jr.; Nelin, C. J.; Laskowski, B. C.; Seel, M. *J. Chem. Phys.* **1984**, *81*, 3594.

(60) Peterson, K. A. In *Correlation consistent basis sets with relativistic effective core potentials. The transition metal elements Y and Hg*; Wilson, A. K., Ed.; ACS Symposium Series: Recent Advances in Electronic Correlation Methodology; American Chemical Society: Washington, DC, in preparation.

(61) Hausserman, U.; Dolg, M.; Stoll, H.; Preuss, H.; Schwerdtfeger, P.; Pitzer, R. M. *Mol. Phys.* **1993**, *78*, 1211.

(62) Dunning, T. H., Jr. *J. Chem. Phys.* **1989**, *90*, 1007.

(63) The general behavior of the correlation-consistent basis sets is typically so systematic for a range of properties such that results from a series of calculations using increasingly larger correlation-consistent basis sets can be extrapolated to the CBS limit using a number of approaches (e.g., see: Feller, D. *J. Chem. Phys*. **1992**, *96*, 6104). As it is unknown whether the CBS extrapolation schemes used for first-, second-, and third-row main group molecules will also be the most appropriate methods for describing basis set behavior for the transition metals, an in-depth extrapolation study is needed prior to general use of an approach. Therefore, we have not extrapolated the results to the CBS limit and, rather, report simply the results of the calculations. As shown in the results herein, the trend seen on going to larger correlation-consistent basis sets is extremely useful even without extrapolation to the CBS limit.

(64) Dunham, J. L. *Phys. Rev.* **1932**, *41*, 721.

(65) Moore, C. E. *Atomic Energy Levels*; United States Department of Commerce, National Bureau of Standards: Washington, DC, 1958; Vol. III.

(66) Condon, E. U.; Shortly, G. H. *The Theory of Atomic Spectra*; Cambridge University Press: Cambridge, U.K., 1951.

(67) Kristyán, S.; Pulay, P. *Chem. Phys. Lett.* **1994**, *229*, 175.

(68) Persson, J.; Taylor, P. R. *Theor. Chem. Acc.* **2003**, *110*, 211.

(69) Boys, S. F.; Bernardi, F. *Mol. Phys.* **1970**, *19*, 553.

(70) van Mourik, T.; Wilson, A. K.; Peterson, K. A.; Woon, D. E.; Dunning, T. H., Jr. In *The Effect of Basis Set Superposition Error (BSSE) on the Convergence of Molecular Properties Calculated with the Correlation Consistent Basis Sets*; Wilson, S. Ed.; Advances in Quantum Chemistry, Quantum Systems in Chemistry and Physics, Part I; Academic Press: New York, 1998.

(71) See, for example: McGlynn, S. P.; Azumi, T.; Kinoshita, M. *Molecular Spectroscopy of the Triplet State*; Prentice Hall: Englewood Cliffs, NJ, 1969.

(72) This conclusion is significant to note in studies such as this one, in which a broad range of methods and basis sets are tested, or in studies in which large model compounds are treated. In such cases, treating spin−orbit coupling is extremely demanding and may not be tractable with the existing computational resources. For purposes of assignment of luminescence bands, a difference of $\sim$1000 cm^{-1} is usually insignificant.

(73) Herzberg, G. *Molecular Spectra and Molecular Structure; Vol. I. Spectra of Diatomic Molecules*; Van Nostrand Reinhold: New York, 1950.

(74) Bagus, P. S.; Viinikka, E.-K. *Phys. Rev. A* **1977**, *15*, 1486.

(75) We used the guess=alter keyword in Gaussian 98 to switch between the $^3\Sigma_u^+$ and $^3\Pi_g$ states. By default, the program calculates the lowest energy triplet state. Misleading spectroscopic results will be obtained if they were based on a curve constructed by plotting the lower energy state at each distance or the curve for the $^3\Pi_g$ state.

(76) Callear, A. B.; Kendall, D. R. *Chem. Phys. Lett.* **1979**, *64*, 401.

(77) Başţuğ, T.; Sepp, W.-D.; Kolb, D.; Fricke, B.; Baerends, E. J.; Te Velde, G. *J. Phys. B* **1995**, *28*, 2325.

(78) Koperski, J.; Atkinson, J. B.; Krause, L. *J. Mol. Spectrosc.* **1998**, *187*, 181.

(79) Burda, J. V.; Zahradník, R.; Hobza, P.; Urban, M. *Mol. Phys*. **1996**, *89*, 425.

(80) See, for example, Table 5 in Omary, M. A.; Webb, T. R.; Assefa, Z.; Shankle, G. E.; Patterson. H. H. *Inorg. Chem*. **1998**, *37*, 1380 and Tables 3 and 4 and Figure 9 in Rawashdeh-Omary, M. A.; Omary, M. A.; Patterson, H. H. *J. Am. Chem. Soc.* **2000**, *122*, 10371.

(81) Cabaud, B.; Hoareau, A.; Melinon, P. *J. Phys. D* **1980**, *13*, 1831. (b) Bréchignac, C.; Broyer, M.; Cahuzac, Ph.; Delacretaz, G.; Labastie, P.; Wöste, L. *Chem. Phys. Lett.* **1985**, *120*, 559. (c) Haberland, H.; Kornmeier, H.; Langosh, H.; Oschwald, M.; Tanner, G. *J. Chem. Soc., Faraday Trans.* **1990**, *86*, 2473. (d) Rademann, K.; Dimopoulou-Rademann, O.; Schlauf, M.; Even, U.; Hensen, F. *Phys. Rev. Lett.* **1992**, *69*, 3208. (e) Haberland, H.; Issendorff, B.; Yufeng, J.; Kolar, T.; Thanner, G. *Z. Phys. D* **1993**, *26*, 8. (f) Lang, B.; Vierheilig, A.; Wiedenmann, E.; Buchenau, H.; Gerber, G. *Z. Phys. D* **1997**, *40*, 1.

(82) Butchard, J. A.; Claridge, R. F. C.; Phillips, L. F. *Chem. Phys. Lett.* **1971**, *8*, 139.

(83) Vogler, A.; Kunkely, H. *J. Organomet. Chem.* **1997**, *541*, 177.

(84) Elbjeirami, O.; Omary, M. A.; Stender, M.; Balch, A. L. *Dalton Trans.* **2004**, 3173.

(85) See, for example: (a) Coppens, P. *Chem. Commun.* **2003**, *12*, 1317. (b) Carducci, M. D.; Pressprich, M. R.; Coppens, P. *J. Am. Chem. Soc.* **1997**, *119*, 2669. (c) Novozhilova, I. V.; Volkov, A. V.; Coppens, P. *J. Am. Chem. Soc.* **2003**, *125*, 1079. (d) Kim, C. D.; Pillet, S.; Wu, G.; Fullager, W. K.; Coppens, P. *Acta Crystallogr.* **2002**, *A58*, 133.

(86) See, for example: (a) Saes, M.; Bressler, C.; Abela, R.; Grolimund, D.; Johnson, S.; Heimann, P. A.; Maged, C. *Phys. Rev. Lett.* **2003**, *90*, 47403. (b) Brown, F. L. H.; Wilson, K. R.; Jianshu, C. *J. Chem. Phys.* **1999**, *111*, 6238.

(87) For a review, see: Zink, J. I.; Shin, K. S. K. In *Molecular Distortions in Excited Electronic States Determined from Electronic and Resonance Raman Spectroscopy*; Volman, D. H., Hammond, G. S., Neckers, D. C., Eds.; Advances in Photochemistry; Wiley: New York, 1991; Vol. 16. For recent examples, see: (a) Bussière, G.; Reber, C.; Neuhauser, D.; Walter, D. A.; Zink, J. I. *J. Phys. Chem. A* **2003**, *107*, 1258. (b) Savoie, C.; Reber, C. *J. Am. Chem. Soc.* **2000**, *122*, 844.

(88) van Zee, R. D.; Blankespoor, S. C.; Zwier, T. S. *J. Chem. Phys.* **1988**, *88*, 4650.

(89) References 2 and 3 in ref 88 initially reported 3.25 Å on the basis of gas-phase viscosity data using an inaccurate D_e value known at the time. It was argued in ref 88 that this should be corrected to 3.70 Å using the correct D_e value.

(90) Ceccherini, S.; Moraldi, M. *Chem. Phys. Lett.* **2001**, *337*, 386.

(91) Zehnacker, A.; Duval, M. C.; Jouvet, C.; Lardeux-Dedonder, C.; Solgadi, D.; Soep, B.; Benoist d'Azy, O. *J. Chem. Phys.* **1987**, *86*, 6565.

(92) Koperski, J.; Atkinson, J. B.; Krause, L. *Chem. Phys. Lett.* **1994**, *219*, 161.

(93) Koperski, J.; Atkinson, J. B.; Krause, L. *Can. J. Phys.* **1994**, *72*, 1070.